Optimising gold nanorod size for maximum photoacoustic response while minimising cell toxicity

Oscar B. Knights, Sunjie Ye, Nicola Ingram, David M. J. Cowell, Alexander F. Markham, Steven Freear, and James R. McLaughlan

Articles you may be interested in

Optimizing gold nanorod volume for minimum cell toxicity and maximum photoacoustic response
The Journal of the Acoustical Society of America **141**, 3459 (2017); 10.1121/1.4987177

Summary of "Statistical learning and data science techniques in acoustics research"
Proceedings of Meetings on Acoustics **30**, 022001 (2017); 10.1121/2.0000571

Algebraic reflections in geometric acoustics
Proceedings of Meetings on Acoustics **30**, 022002 (2017); 10.1121/2.0000621

An assessment of two popular Padé-based approaches for fast frequency sweeps of time-harmonic finite element problems
Proceedings of Meetings on Acoustics **30**, 022003 (2017); 10.1121/2.0000649

How understanding and addressing the concerns of women students benefits all students
Proceedings of Meetings on Acoustics **30**, 025004 (2017); 10.1121/2.0000586

Photoacoustic imaging of early inflammatory response using gold nanorods
Applied Physics Letters **90**, 223901 (2007); 10.1063/1.2743752

Optimising gold nanorod size for maximum photoacoustic response while minimising cell toxicity

Oscar B. Knights
School of Electronic and Electrical Engineering, University of Leeds, Leeds, LS2 9JT, UNITED KINGDOM; elok@leeds.ac.uk

Sunjie Ye
Leeds Institute of Biomedical and Clinical Sciences, Leeds, UNITED KINGDOM; S.Ye@leeds.ac.uk

Nicola Ingram
Leeds Institute of Biomedical and Clinical Sciences, University of Leeds, Leeds, LS2 9JT, UNITED KINGDOM; N.Ingram@leeds.ac.uk

David M. J. Cowell
University of Leeds, Leeds, UNITED KINGDOM; D.M.J.Cowell@leeds.ac.uk

Alexander F. Markham
Leeds Institute of Biomedical and Clinical Sciences, University of Leeds, Leeds, LS2 9JT, UNITED KINGDOM; A.F.Markham@leeds.ac.uk

Steven Freear and James R. McLaughlan
University of Leeds, Leeds, UNITED KINGDOM; s.freear@leeds.ac.uk, J.R.McLaughlan@leeds.ac.uk

Plasmonic nanoparticles show great potential for molecular-targeted photoacoustic (PA) imaging. To maximise light absorption, the gold nanorods (AuNRs) are illuminated at their surface plasmon resonance (SPR), which for biomedical application is typically in the 'optical window' of 700-900nm. For AuNRs, one of the main factors that determines the SPR is their aspect ratio. Since it is possible to have a similar aspect ratio, but different size of the particle the choice of particle could have a critical effect on a number of factors, such as, photoacoustic emissions, cell toxicity and therapeutic efficacy. For example, a particular sized AuNR may produce a higher PA response, for an equivalent laser fluence, but be more toxic to cell populations. In this study, the PA response of AuNRs with four different volumes but similar aspect ratios (~4) are compared. A linear relationship between incident laser fluence and PA amplitude is shown and results indicate that AuNRs with larger volumes produce stronger PA emissions. In-vitro cell studies were performed on a lung cancer cell line to assess the cell toxicity of the different sized AuNRs via a colourmetric assay.

Name	Width	Length	Aspect Ratio	SPR
Au10	9.9 ± 1.1 nm	39.7 ± 5.4 nm	3.98 ± 0.51	811 ± 2 nm
Au25	23.2 ± 2.6 nm	85.6 ± 9.8 nm	3.73 ± 0.63	803 ± 2 nm
Au40	39.8 ± 4.1 nm	122.5 ± 13.8 nm	3.10 ± 0.35	790 ± 2 nm
Au50	42.2 ± 4.6 nm	142.0 ± 17.0 nm	3.38 ± 0.41	841 ± 2 nm

Table 1: Size distributions and SPRs of the AuNRs used in the study, determined by TEM analysis and spectrophotometry respectively. The uncertainty of measurement is the standard deviation of the sample.

1. INTRODUCTION

Gold nanorods (AuNRs) possess particular characteristics that enable them to be used in biomedical applications such as photoacoustics (PA) and photothermal therapy.[1] Examples of these remarkable properties include tuneable surface plasmon resonances (SPRs),[2] potential for functionalisation,[3,4] relative biocompatibility[5,6] (partly due to gold being chemically inert), and high colloidal stability.[7,8] By altering the aspect ratio of the AuNRs, their peak SPR can be tuned to absorb strongly in the near-infrared wavelength range - a region known as the 'biological window' since reduced optical absorption in biological tissues is observed.[9,10] Considering that the AuNRs can be many different sizes while maintaining a similar aspect ratio (and therefore SPR), the size of the AuNRs may have an affect on a number of areas related to how they are used. For example, in photoacoustic imaging, the size of AuNRs may significantly impact on the optoacoustic conversion efficacy which will in turn affect the final outcome. There may also be other important size-dependent relationships, such as energy thresholds for melting and reshaping, and AuNR toxicity to cell populations, both of which are crucial aspects to consider if AuNRs are to be used clinically.[11] For instance, if a certain laser fluence was required to generate a sufficient PA response but the AuNRs being employed were susceptible to melting at these fluences, then they may melt before the desired outcome has been achieved. The aim of this study is to measure and evaluate the effects that AuNR size has on a number of important factors relating to PA imaging, namely their PA emission amplitudes, melting and reshaping fluence thresholds, toxicity to cell populations, and cellular uptake.

2. MATERIALS AND METHODS

A. GOLD NANORODS

Citrate-capped AuNRs with certified widths of 10 nm, 25 nm, 40 nm, and 50 nm, and similar SPRs were purchased (A12, Nanopartz, USA) to be the source of the photoacoustic signals. This enabled a comparison to be made between the different sized AuNRs and their corresponding PA signals, melting and reshaping thresholds, cell toxicity, and cellular uptake, while maintaining similar aspect ratios. For clarity, the AuNRs will be named Au10, Au25, Au40, and Au50, where the number refers to the certified width of the AuNRs. Transmission electron microscope (Tecnai[TM] TF20, FEI, USA) images were taken (200 kV accelerating voltage) and analysed to determine the size distributions of the AuNRs, and spectrophotometry was used to establish the peak SPR of each AuNR size (shown in Table 1). The normalised absorbance spectra of each AuNR size is shown in Fig. 1a.

B. PHOTOACOUSTICS

The experimental setup for the detection of PA signals from the AuNRs is shown in Fig. 2. A pulsed tuneable laser system (Surelite[TM] OPO Plus, Continuum[®], USA) was used to generate a PA response from
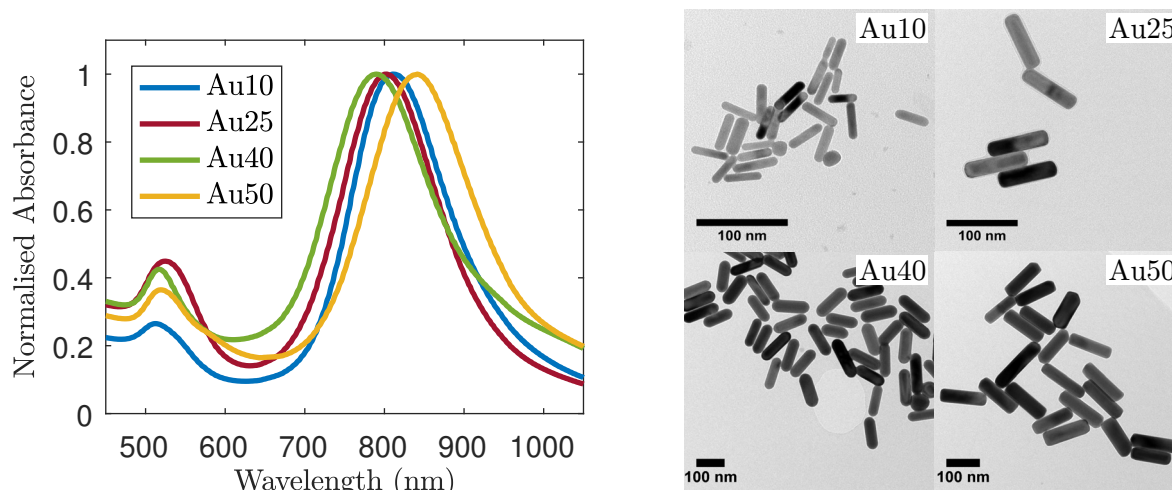
Figure 1: (a) Normalised absorbance spectra of the Au10s, Au25s, Au40s, and Au50s, displaying peak surface plasmon resonance at $811 \pm 2\,nm$, $803 \pm 2\,nm$, $790 \pm 2\,nm$, and $841 \pm 2\,nm$, respectively. (b) Transmission electron microscope images of Au10 (top-left), Au25 (top-right), Au40 (bottom-left), and Au50 (bottom-right). Scale bar = 100 nm
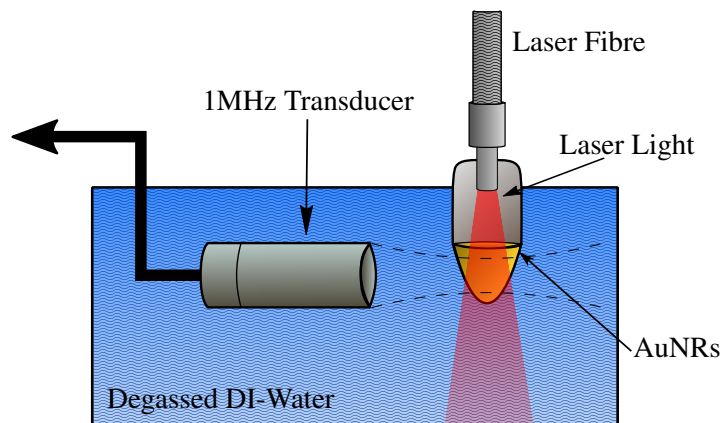

Figure 2: Experimental setup used to detect the photoacoustic response of AuNRs.

the AuNRs operating at 10 Hz with a pulse width of 7 ns and spot size of 5 mm at the target region. The PA signals were detected using a focussed 1 MHz single-element transducer (V303, Olympus, UK), aligned to the centre of the absorbing region. The signals were recorded with a data acquisition (DAQ) card (M4i.4420x8, Spectrum, Germany) after being subject to 40 dB amplification via a pre-amplifier (SPA.1411, Spectrum, Germany).

For each set of photoacoustic measurements, a suspension of AuNRs was made to the desired concentration by diluting the original stock solution with deionised water. The new AuNR suspension was then agitated in an ultrasound bath for 15 min to reduce aggregation and ensure a uniform distribution of AuNRs before being placed inside a small plastic container (Eppendorf, Germany) for PA signal measurements. The laser wavelength was tuned to the exact SPR of each AuNR type (Table 1), measured via spectrophotometry (Fig. 1a), to maximise the optical absorption exhibited by the AuNRs. As a consequence of this, the energy of 100 laser pulses was measured at each wavelength studied, and the laser output was adjusted to ensure that equivalent laser fluences were used across all AuNRs.
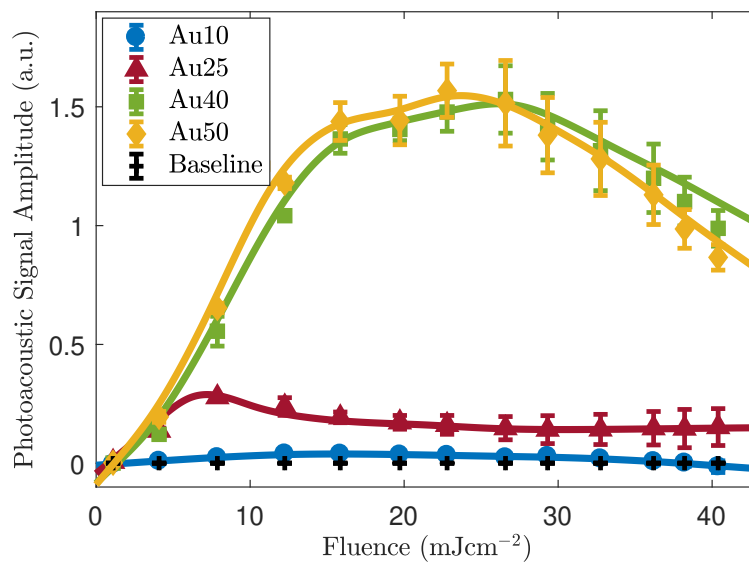
Figure 3: Photoacoustic amplitude of each sized AuNR as a function of incident laser fluence.

The PA signal emitted by each AuNR type was recorded across a range of incident laser fluences from approximately $1 - 40 \, \mathrm{mJ \, cm^{-2}}$ in steps equivalent to 4 % of the highest fluence studied. The AuNRs were exposed to 20 laser pulses at each laser fluence, and the subsequent PA signals were recorded and averaged to obtain a single PA measurement. It was decided that 20 laser pulses were required to account for the small fluctuations in the laser output energy and also to increase the signal-to-noise ratio of the waveforms. The whole process was repeated three times on fresh samples for reproducibility. In addition, PA signals were also recorded from the container (filled with DI-water instead of AuNRs) and also while the laser was firing but with the shutter closed (i.e. no light was incident on the target). These signals were recorded under the exact same conditions as the AuNRs.

To calculate the PA signal amplitude, the recorded signals were first windowed to a 7 μs region. A Hilbert transform was then applied to the shortened signal and the amplitude was calculated by integrating across the envelope of the signal. To account for effects of the container, the PA amplitude of the signal that was recorded with a water-filled container was removed from the original AuNR PA amplitude to obtain a corrected value. The three sets of repeat data on fresh samples were averaged to obtain a single PA amplitude and the standard error of the mean was calculated. A baseline noise amplitude was also calculated for reference.

C.   GOLD NANOROD TOXICITY & CELLULAR UPTAKE

The toxicity of the four AuNR sizes to a non-small cell lung cancer cell line (A549, ATCC, UK) was investigated via a 72 h MTT (3-[4,5-dimethylthiazol-2-yl]-2,5 diphenyl tetrazolium bromide) colorimetric assay. The lung cancer cells were cultured in DMEM (Dulbecco's Modified Eagle Medium) medium supplemented with 10 % FBS (Fetal Bovine Serum) until they reached 80 % confluency. A 96-well plate was seeded with 1×10^3 cells per well and incubated for 24 h before each type of AuNRs was added at a maximum concentration of $3 \times 10^{10} \, \mathrm{NP \, ml^{-1}}$ with each subsequent column receiving a 1:3 series dilution. Following 72 h incubation, the AuNR-medium in each well was replaced with an MTT-medium solution at a concentration of $500 \, \mathrm{\mu g \, ml^{-1}}$ and further incubated for 3 h to allow any active cells to metabolise the MTT. Finally, the MTT-medium solution was removed from each well, and the plate was wrapped in foil
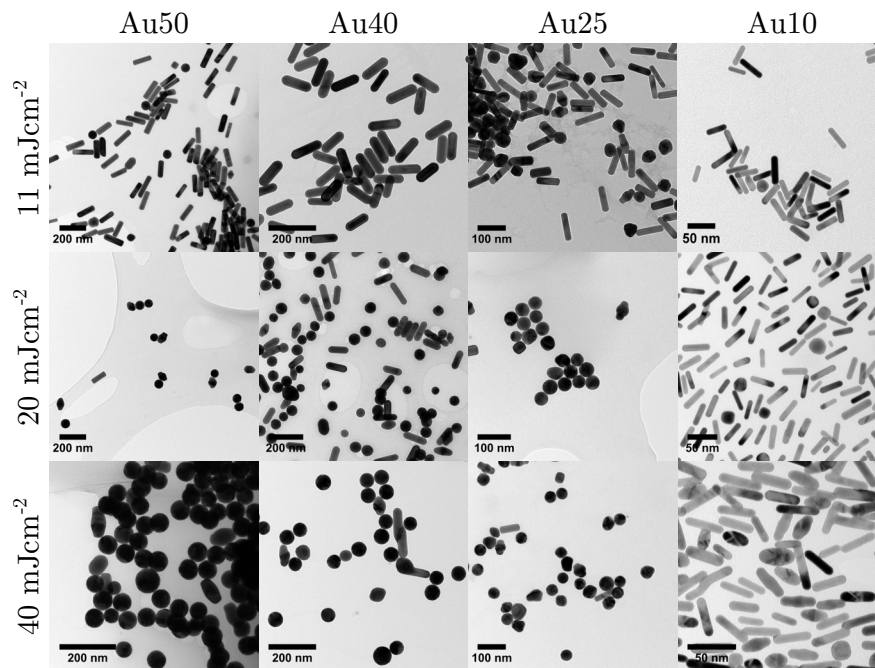
Figure 4: Transmission electron microscope images of all AuNR sizes after 20 laser pulses with a fluence of 11 mJ cm^{-2} (top row), 20 mJ cm^{-2} (middle row), and 40 mJ cm^{-2} (bottom row).

and stored at approximately 4 °C, ready for the absorbance to be measured with a plate reader (Mithras LB 940, Berthold Technologies, Germany) at a further date.

To calculate the cell viability as a function of AuNR concentration, the absorbance values from each well of the 96-well plate were averaged per column and the background absorbance value (with cells only) was subtracted to obtain a corrected value. The cell viability was finally calculated by the ratio of mean absorbance of the sample with respect to mean absorbance of the control group (cells with Dulbecco's Phosphate-Buffered Saline (DPBS) only). This method was repeated three times on fresh samples to enable a mean cell viability to be determined.

Dark-field microscopy was used to provide an indication of the size-dependent cellular uptake of AuNRs. The A549 cells were plated onto 22×22 mm glass coverslips at a density of 1×10^5 well^{-1} and incubated for two days before replacing the medium with an AuNR-medium solution at a concentration of 1×10^{11} NP ml^{-1}. After a further 4 h incubation, the medium containing AuNRs was removed from each well, and the coverslips were washed twice with DPBS. A 4 % paraformaldehyde/DPBS solution was then added to the wells to allow the cells to fix to the coverslip, and after a 10 min period at room temperature, the coverslips were washed twice with DPBS ready for imaging. Both the bright and dark-field images were taken with an optical microscope (Nikon Eclipse Ti-E, Nikon UK Ltd, UK) at 100x magnification.

3.   RESULTS AND DISCUSSION

The relationship between incident laser fluence and PA emission amplitude for all four AuNR types is shown in Fig. 3. The data clearly show a relationship between AuNR size and PA amplitude, where the larger AuNRs display a significantly larger PA response compared with the smaller AuNRs. Although difficult to see for the Au10s, at relatively low fluences all four AuNR types exhibit a linear PA response with respect to incident fluence, as expected. However, the maximum PA amplitude displayed by the different sized AuNRs varies considerably. The Au50s produced the largest photoacoustic response, at the respective
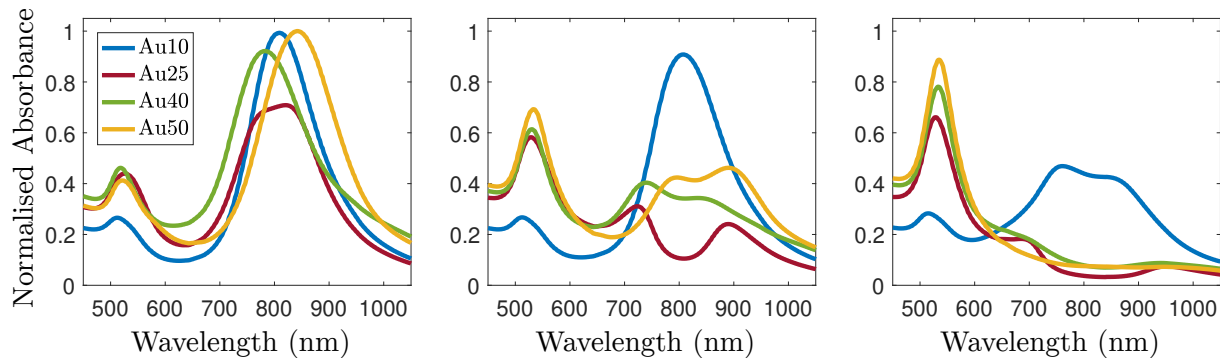
Figure 5: Normalised absorbance spectra of all AuNR sizes after 20 laser pulses with a fluence of 11 mJ cm^{-2} (left), 20 mJ cm^{-2} (middle), and 40 mJ cm^{-2} (right).

laser fluence, with a maximum PA amplitude that is more than a factor of 38 times larger than that of the Au10s, and more than 5 times larger than that of the Au25s. The quoted PA amplitudes are at their respective fluence levels and not at an equivalent fluence level, however this is justified since the laser parameters would be optimised to match that of the AuNRs being utilised in a real-world environment. It is also worth noting here that all the quoted fluence levels are well below the maximum permissible exposure for skin of a single laser pulse at 810 nm (approximately 33 mJ cm^{-2}).

It is clear from the data that the different sized AuNRs begin to lose their linear PA relationship at different points, and this loss of linearity potentially indicates the melting or reshaping of the AuNRs since this would cause a significant reduction in their absorbance. Interestingly, the Au25s are the first to lose linearity at approximately 7 ± 1.9 mJ cm^{-2}, followed by the Au10s at $12 - 14 \pm 2$ mJ cm^{-2}, and finally the Au40s and Au50s both become non-linear around $14 - 16 \pm 2.2$ mJ cm^{-2}. Statistical significance ($p < 0.05$) was established for all quoted fluence levels. To test the hypothesis that the reduction in PA amplitude at higher fluences was due to melting, TEM images and absorbance spectra were taken on fresh samples of AuNRs at key fluences along the curve: 11 mJ cm^{-2}, 20 mJ cm^{-2}, and 40 mJ cm^{-2}, shown in Fig. 4 and 5. After 20 laser pulses at 11 mJ cm^{-2}, the Au25s show a significant reduction in the peak absorbance, and the TEM images show that a large percentage of AuNRs have indeed melted and reshaped. The rest do not display any significant reduction at this fluence. When the fluence is increased to 20 mJ cm^{-2}, the Au25s, Au40s, and Au50s all display a considerable reduction in absorbance at their longitudinal SPR band, with the Au25s exhibiting a large 'hole' in their absorbance spectrum. Surprisingly, the Au10s appear to remain relatively stable as the absorbance shows little decline. Again, the TEM images confirm these findings, where the smallest AuNRs show little melting, and the other three sizes demonstrate a large proportion of AuNRs having reshaped into spheres. Finally, at a fluence of 40 mJ cm^{-2}, all four AuNR sizes display a major recession in their longitudinal SPR, however the Au10s still retain almost half of their original absorbance. The melting resistance of the Au10s may be explained by their heightened thermal coupling to the surrounding medium resulting in rapid cooling of the AuNRs and therefore not melting into complete spheres. The TEM images support this hypothesis since a large number of the AuNRs appear to be elliptical or $\phi-$shaped. In addition to the reduction in the longitudinal SPR band of all four AuNR sizes, there is also an increase in the latitudinal SPR band, as the laser fluence is increased (as can be seen in Fig. 5). This is due to the melting of the rod-shaped gold particles into spherical particles, which have a single plasmon band at 532 nm. The Au10s are the only AuNRs not to display any significant change in the 532 nm band, and this supports the previous idea that the AuNRs are not melting fully into spheres, and are instead forming into imperfect spheres and other non-spherical shapes.

While the size-dependent PA relationship of the AuNRs is important to understand, consideration must
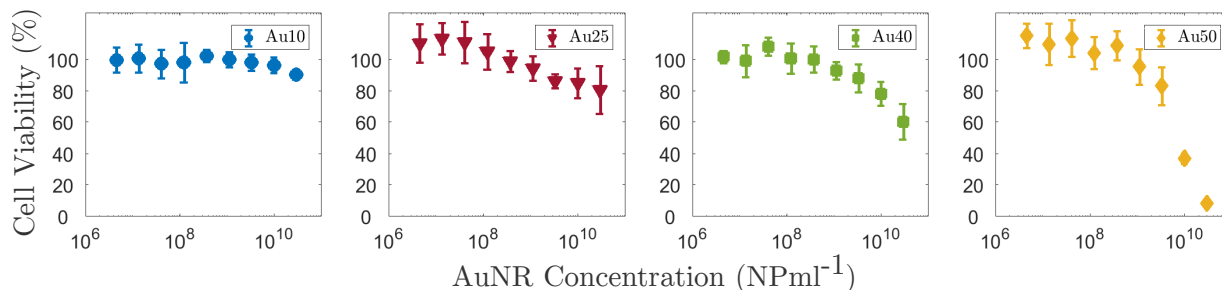
Figure 6: Percentage cell viability of a lung cancer cell line incubated with four different sized AuNRs, measured across a range of concentrations (1:3 series dilution) with a maximum concentration of $3 \times 10^{10}\,NP\,ml^{-1}$, as determined by a 72 h MTT assay.
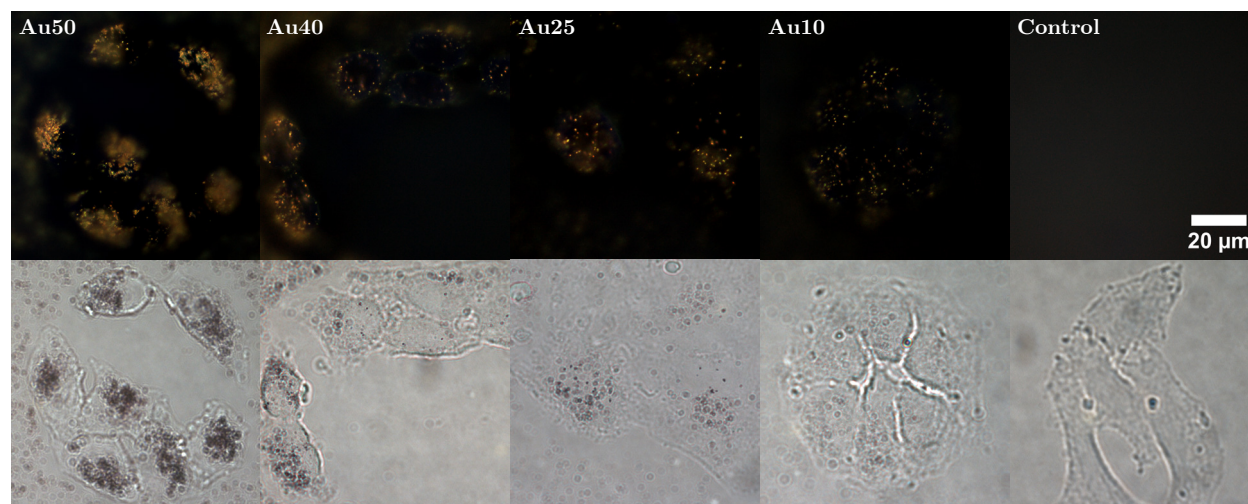

Figure 7: Bright- and Dark-field microscopy images of a lung cancer cell line incubated with four differ-ent sized AuNRs at a concentration of $1 \times 10^{11}\,NP\,ml^{-1}$.

also be made with regards to their cytotoxicity. If a certain sized AuNR produces an optimal PA response but is highly toxic to cell populations, then it may not be the best choice of particle. Thus, the toxicity of the four different sized AuNRs to a non-small cell lung cancer cell line (A549) was studied. The results of the MTT assay are shown in Fig. 6, where a size-dependent relationship is evident. The cell viability of the two smaller AuNRs (Au10s and Au25s) remained high across all concentrations studied, indicating no significant toxicity, however the Au40s and Au50s displayed considerable toxicity at the higher con-centrations. A four-parameter logistic regression curve was fitted to the data for the two larger AuNRs (Au40s and Au50s) to determine an LD_{50} value[12] - a value that indicates the required concentration of a substance that results in 50 % cell death. The Au40s and Au50s exhibited an $LD_{50} = 6.6 \times 10^{10}\,NP\,ml^{-1}$ and $LD_{50} = 7.3 \times 10^{9}\,NP\,ml^{-1}$, respectively.

In addition to understanding toxicity, the cellular uptake of the AuNRs was investigated using dark-field microscopy. Figure 7 shows bright- and dark-field microscopy images of the same lung cancer cell line, incubated with AuNRs. The images suggest that the AuNRs are distributed in the cytoplasm of the cells, instead of randomly or evenly distributed (which would be the case of non-specific adhesion). It also appears that the larger AuNRs have been taken up more preferentially than the smaller AuNRs, since a stronger signal is observed from the larger AuNRs. This increase in AuNR uptake may also explain the higher toxicity levels exhibited by the larger AuNRs.

4. CONCLUSIONS

The size of the AuNRs that are utilised for use in biomedical applications has a substantial effect on a large number of parameters, such as photoacoustic amplitude, reshaping fluence thresholds, and cellular toxicity and uptake; and if they are to be used in the clinical setting, understanding these size-dependent effects is crucial to their development. It is suggested that there may be an optimal sized AuNR for use in PA imaging. Larger AuNRs were shown to produce stronger PA emission amplitudes but also exhibited the greatest cellular toxicity and uptake. Conversely, the smaller AuNRs produced the weakest PA emissions but were the least toxic to the lung cancer cell line, and the smallest of the four AuNRs studied (Au10s) indicated the highest photostability.

ACKNOWLEDGEMENTS

REFERENCES

[1] Keisuke Nakayama, Katsuaki Tanabe, and Harry A Atwater. Plasmonic nanoparticle enhanced light absorption in gaas solar cells. *Applied Physics Letters*, 93(12):121904, 2008.

[2] Nikolai G Khlebtsov and Lev A Dykman. Optical properties and biomedical applications of plasmonic nanoparticles. *Journal of Quantitative Spectroscopy and Radiative Transfer*, 111(1):1–35, 2010.

[3] Dakrong Pissuwan, Stella M Valenzuela, Catherine M Miller, and Michael B Cortie. A golden bullet? selective targeting of toxoplasma gondii tachyzoites using antibody-functionalized gold nanorods. *Nano letters*, 7(12):3808–3812, 2007.

[4] Tanya S Hauck, Arezou A Ghazani, and Warren CW Chan. Assessing the effect of surface chemistry on gold nanorod uptake, toxicity, and gene expression in mammalian cells. *Small*, 4(1):153–159, 2008.

[5] J.A. Khan, B. Pillai, T.K. Das, Y. Singh, and S. Maiti. Molecular effects of uptake of gold nanoparticles in hela cells. *ChemBioChem*, 8(11):1237–1240, 2007.

[6] E.E. Connor, J. Mwamuka, A. Gole, C.J. Murphy, and M.D. Wyatt. Gold nanoparticles are taken up by human cells but do not cause acute cytotoxicity. *Small*, 1(3):325–327, 2005.

[7] Guodong Zhang, Zhi Yang, Wei Lu, Rui Zhang, Qian Huang, Mei Tian, Li Li, Dong Liang, and Chun Li. Influence of anchoring ligands and particle size on the colloidal stability and in vivo biodistribution of polyethylene glycol-coated gold nanoparticles in tumor-xenografted mice. *Biomaterials*, 30(10):1928–1936, 2009.

[8] Vivek Sharma, Kyoungweon Park, and Mohan Srinivasarao. Colloidal dispersion of gold nanorods: Historical background, optical properties, seed-mediated synthesis, shape separation and self-assembly. *Materials Science and Engineering: R: Reports*, 65(1):1–38, 2009.

[9] Yuanfu Huang, Kai Xia, Nongyue He, Zhuoxuan Lu, Liming Zhang, Yan Deng, and Libo Nie. Size-tunable synthesis of gold nanorods using pyrogallol as a reducing agent. *Science China Chemistry*, 58(11):1759–1765, 2015.

[10] A. Bouhelier, R. Bachelot, G. Lerondel, S. Kostcheev, P. Royer, and G. P. Wiederrecht. Surface plasmon characteristics of tunable photoluminescence in single gold nanorods. *Phys. Rev. Lett.*, 95:267405, Dec 2005.

[11] Oscar B. Knights, David Cowell, James R. McLaughlan, and Steven Freear. Optimizing gold nanorod volume for minimum cell toxicity and maximum photoacoustic response. *The Journal of the Acoustical Society of America*, 141(5):3459–3459, 2017.

[12] Giuseppe Cardillo. Four parameters logistic regression - there and back again (version 1.1) [matlab code]. Available at https://uk.mathworks.com/matlabcentral/fileexchange/38122-four-parameters-logistic-regression-there-and-back-again (Accessed 02 May 2017), 2012.